Controlled Suppression of Wear on the Nanoscale by Ultrasonic Vibrations

Patricia Pedraz,[†] Reinhold Wannemacher,[*,†] and Enrico Gnecco[*,†,‡]

[†]IMDEA Nanociencia, Campus Universitario de Cantoblanco, Calle Faraday 9, 28049 Madrid, Spain and [‡]Otto Schott Institute of Materials Research (OSIM), Friedrich Schiller University Jena, 07743 Jena, Germany

ABSTRACT Wear on the nanoscale, as evidenced by the formation of periodic ripples on a model polystyrene thin film while a sharp tip is sliding on it with a normal force in the μN range, is shown to be suppressed by the application of ultrasonic vibrations of amplitude A_{exc}. An accurate calibration of the transducer excitation amplitude is achieved by a home-built setup based on a laser Doppler vibrometer. The corrugation of the typical ripple pattern that is formed in the absence of vibrations is reduced when the excitation frequency matches the contact resonance of the system and A_{exc} progressively increases. Above a critical value of A_{exc}, the ripples completely disappear, while the friction levels off at a finite value determined by the normal force and the vibration amplitude. This value can be significantly smaller than the value of the macroscopic friction coefficient. In addition to the control of wear in general, this opens up the possibility of controlled nanolithography with improved accuracy.

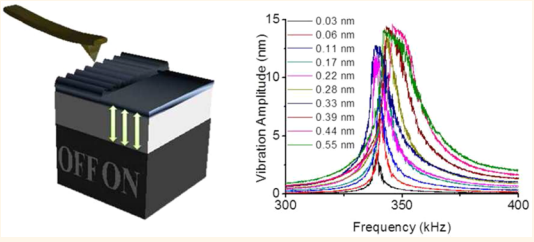

KEYWORDS: friction · wear · ultrasonic vibrations · AFM · polymers

The development of novel approaches for reducing wear on the nanoscale is an important issue for proper functioning of micro- and nanoelectromechanical systems (MEMS and NEMS). In these cases, traditional lubricants cannot be used since their viscosity dramatically increases when molecular chains are confined into nanometer-sized interstices.[1] At the macroscopic scale and, in particular, for technical purposes, sonic and ultrasonic vibrations have been used for many years to modify frictional behavior to reduce wear and also undesired acoustic emission due to friction in industrial processes.[2−5] Reduction of the coefficient of static as well as of sliding friction up to 100% was observed experimentally.[6] Typically, friction is described as being caused by elastic and plastic deformation of microscopic asperities of the sliding surfaces, the true contact area being 3 or 4 orders of magnitude less than the macroscopic surface area.[7] Friction reduction due to normal vibration is then thought to be caused by slip during the phase of decompression of the contacts, whereas the surfaces stick during the compressional phase.[8] For a recent review of the field, see ref 9, for example.

On a microscopic scale, Hesjedal and Behme[10] investigated the friction reduction in the microscopic contact of an atomic force microscope (AFM), when surface acoustic waves (SAWs) were excited on the surface of the sample. The frequencies of these waves varied between 200 MHz and 3 GHz, and various hard materials were studied, such as quartz, GaAs, AlN, $LiTaO_3$, SiO_2, Al, Au, and Ni. Only the normal component of the vibrations was found to be responsible for friction reduction in these experiments. Friction on the atomic scale was investigated later, in ultrahigh vacuum (UHV),[11−13] where a significant reduction of friction was observed when bending or torsional mechanical resonances between the AFM tip and alkali halide surfaces were excited at much lower frequencies (20−300 kHz). Following this strategy, prevention of abrasive wear of a silicon tip sliding over several hundred meters was demonstrated by Lantz *et al.*[14]

In the present work, we investigate the effect of mechanical vibrations on wear on the nanoscale and select for this purpose the formation of ripples as a typical form of wear, which is often observed on microscopic as well as macroscopic length scales, in particular on the surface of compliant materials.[15] On the nanoscale, ripples have been frequently observed on polymer surfaces,[16,17] usually after repeated scanning of

* Address correspondence to reinhold.wannemacher@imdea.org, enrico.gnecco@imdea.org.

Received for review April 24, 2015 and accepted August 21, 2015.

Published online August 24, 2015
10.1021/acsnano.5b02466

the same area[16,18] or working above their glass transition temperature.[19] However, more recently it was shown that ripples can also be formed on the surface of a spin-coated thin film of solvent-enriched polystyrene (PS) in a single scan when scanning the sample in contact mode with a sharp tip at ambient conditions.[20] Here we show how these ripples disappear when vertical vibrations are applied to the sample at the contact resonance frequency (f_{res}) of the tip of an AFM in contact with the sample with a well-defined amplitude (A_{exc}). We also report a reduction in friction to values smaller than those corresponding to the macroscopic friction coefficient.

RESULTS

In the present study, external mechanical vibrations are induced by a piezoelectric transducer coupled to the sample at frequencies around the lowest bending resonance frequency of the cantilever in contact with the sample (see Experimental Setup). In Figure 1A,B, the contact resonance peak, as seen in the vertical deflection, is shown for different excitation amplitudes and for loads of 26 nN (A) and 442 nN (B). The contact resonance frequency shifts to higher frequencies with increasing load. At the same time, the width of the resonance curves decreases with increasing load and increases with increasing vibration amplitude. This is in accordance with previous reports.[21,22] For higher amplitude values, the peak becomes asymmetric and shifts due to the nonlinear behavior described in refs 23 and 24 The quality factor (Q) decreases with increasing A_{exc}, as seen in Figure 1C (left-hand scale), independent of the load. The vibration amplitude, A_{vib}, as determined by the calibrated vertical sentivity of the quadrant photodiode, rises with A_{exc} and saturates at higher drive amplitudes at about 11 nm for a load of 479 nN, as indicated in Figure 1C (right-hand scale). Here, we have used the standard static calibration of the vertical tip deflection as we did not attempt to interferometrically calibrate the vibration of the cantilever itself. Because under conditions of resonance the vibration amplitude is large compared with the excitation amplitude, $A_{exc} \ll A_{vib}$, and because the elastic modulus of silicon (about 150 GPa[25] depending on the crystalline orientation and the kind of applied stress) is very large compared with the one of polystyrene (about 3.5 GPa[26]), the cantilever deflection is almost entirely due to deformation of the sample. Moreover, it is interesting to observe that, at the contact resonance, A_{vib} corresponds to a normal velocity amplitude on the order of several millimeters per second (for example, f_{res}= 360 kHz, A_{exc} = 10 nm yields $v_{normal} = 2\pi f_{res} A_{exc}$ = 23 mm/s, that is, 3 orders of magnitude larger than the scan velocity (10 μm/s employed in the experiments described). The effect of the contact resonance consists only in the resonant enhancement of the vibration amplitude, so it is expected to see ripples disappear at other drive frequencies but at correspondingly higher drive amplitudes. The measured vibration amplitudes at the maximum excitation amplitude employed, A_{exc} = 0.55 nm, initially increase with the load (see Figure 1D), and at values exceeding ~200 nN, they scatter significantly. We tentatively ascribe this

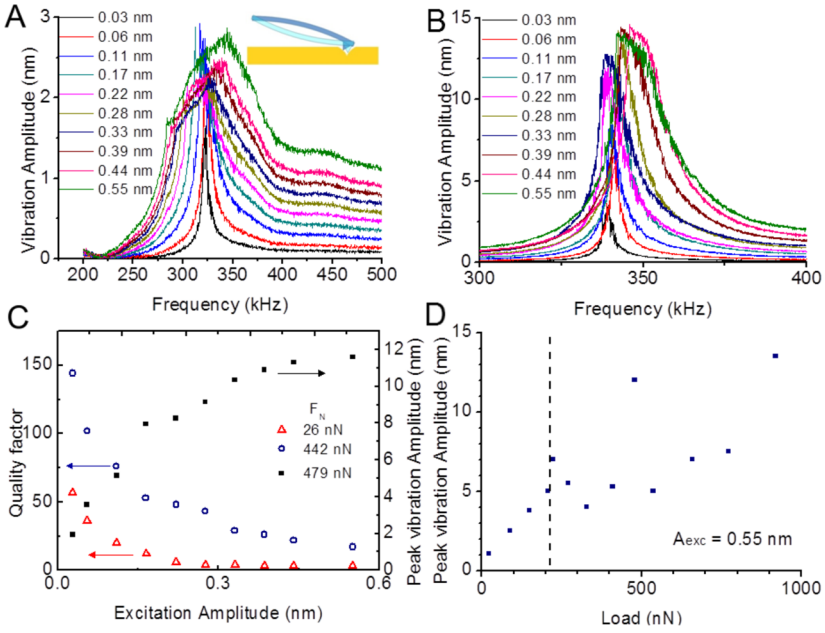

Figure 1. (A) Contact resonance spectra at different ultrasonic excitation amplitudes on the PS sample measured when applying a static load of 26 nN. The free resonance of the cantilever is 71.6 kHz. (B) Same for a static load of 442 nN. Different scales for the abcissa in panels A and B should be noticed. (C) Quality factor *Q versus* A_{exc} at two different loads (left axis) and peak vibration amplitude (right axis), as obtained using the standard static calibration of the vertical deflection *versus* A_{exc} at 479 nN. (D) Peak vibration amplitude at A_{exc} = 0.55 nm versus load. All data points were acquired on different spots of the sample.

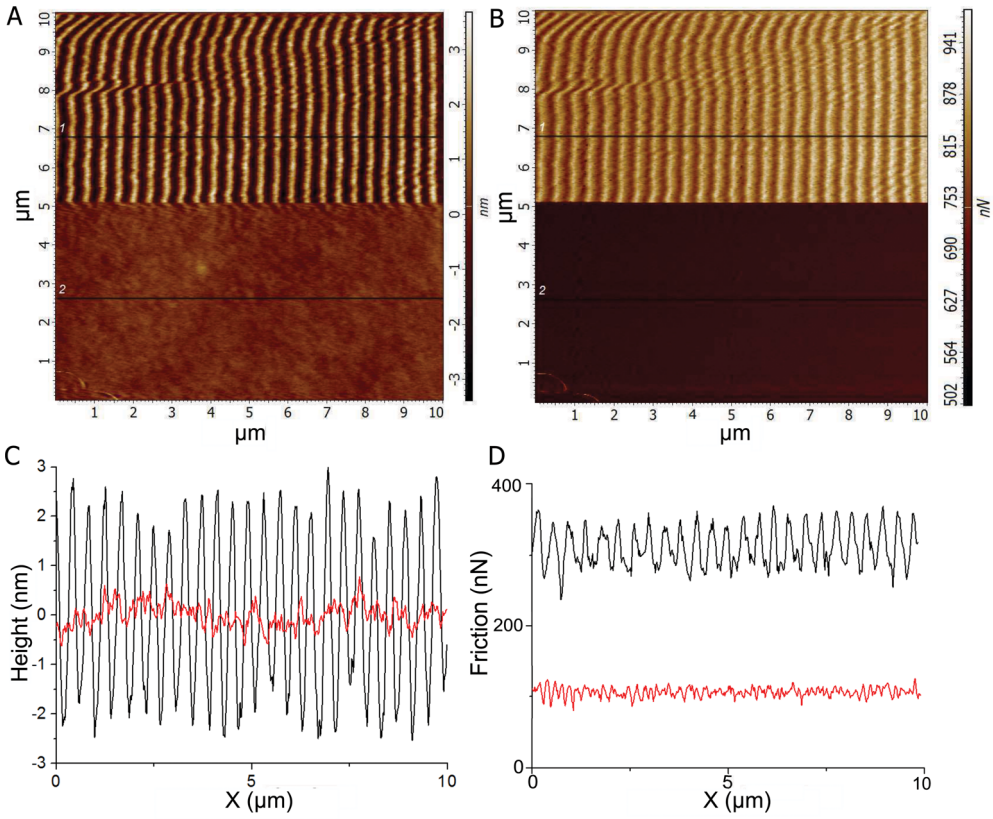

Figure 2. Topography (A) and lateral force (retrace, B) maps and profiles corresponding to the black lines (C and D) while scanning in contact mode (static load 1378 nN). An ac voltage of peak amplitude 10 V ($10V_p$) at 366 kHz was applied to the transducer while acquiring the lower parts of the images, corresponding to a peak excitation amplitude of 0.55 nm (red profile). The drive voltage was zero while acquiring the upper parts of the image (black profile).

behavior to the onset of plastic deformation, which implies hysteresis and therefore dependence of the response on the history of the sample under the tip (compare the discussion below).

When the sample is scanned with the tip, external vertical vibrations with frequency in the vicinity of f_{res} have a clear effect on wear of the PS surface and on friction between the tip and the sample, even at small transducer oscillation amplitudes below 1 nm. This is demonstrated in Figure 2. In the absence of mechanical vibrations (upper part of the figure), a ripple pattern is observed. The ripples disappear immediately when, during the acquisition of the image, the piezoelectric transducer starts vibrating with a peak amplitude of 0.55 nm ($10V_p$ applied ac voltage) at $f = f_{res}$. At the same time, friction is noticeably reduced by a factor of 3. Note that the friction is obtained in the standard way as the difference of lateral force values in the trace and retrace images divided by two. Wear in the form of ripple formation can be considered as a prestage of abrasive wear.[15] Therefore, it is expected that also abrasive wear will be reduced by external vibrations, but we have not studied this regime of even higher normal forces here.

We have also investigated how the amplitude of the normal vibration of the piezoelectric transducer and, hence of the sample surface, influences both ripple formation and friction between tip and sample. To get a quantitative picture of this effect, we have repeated the measurements corresponding to Figure 2 at different excitation amplitudes and calculated the fast Fourier transform (FFT) of the topography line by line. Figure 3 shows the results of such an analysis. At low A_{exc} (Figure 3A), there is no significant change in periodicity and corrugation of the ripples along the scan whether or not the vibration is present. Here, as elsewhere in the paper, the corrugation is defined as the magnitude of the lowest-order Fourier component of the topography representing the ripples. At high A_{exc} (Figure 3C), ripples disappear as soon as the vibration starts. However, at intermediate amplitudes (Figure 3B), we observe a transition stage where ripples become less pronounced, and periodicity and corrugation decreases. The duration of the transition stage is shorter when the vibration amplitude is larger. It is interesting to note that ripples disappear as soon as the plateau value of about 10 nm for the amplified vibration amplitude (as shown in Figure 1C) is reached. The presence of the transition stage from the stick–slip movement without external vibrations to a smooth movement after turn-on of vibrations with small amplitudes is presumably due to overlap with previous scan lines where ripples exist. It should be noted here that the distance between scan lines is only 20 nm.

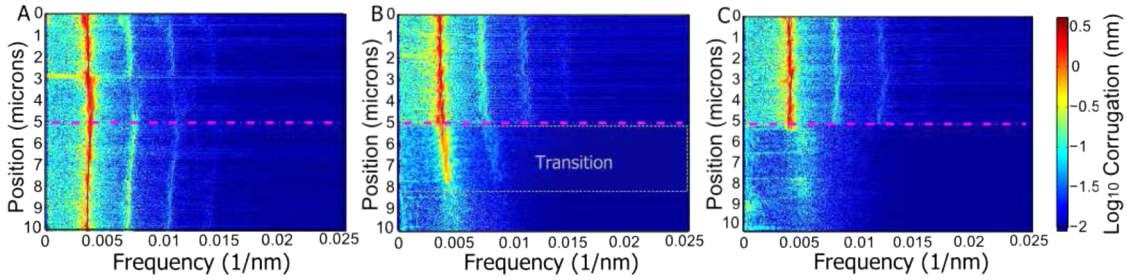

Figure 3. (A) FFT of ripple corrugation along fast scan direction, in nm, on a logarithmic scale (colorbar) for A_{exc} = 0.03 nm (0.5V_p) at the contact resonance frequency. Vertical axis corresponds to slow scan direction. (B) Same for an excitation amplitude of 0.22 nm (4V_p). (C) Same for A_{exc} = 0.55 nm (10V_p). Magenta dashed lines in slow scan direction show the scan line where the vibration is turned on. Applied static load is 442 nN. In each image, vibration is induced at the f_{res} obtained for the determined load and for the chosen excitation amplitude.

This overlap stabilizes the stick−slip movement until the corrugation is gradually reduced and the ripples disappear. In the case of larger excitation amplitudes, the transition stage is correspondingly shorter.

Next, AFM images in contact mode of pristine sample areas were acquired while sweeping the frequency of the external vibration around f_{res} = 362 kHz. Figure 4A,B shows the corresponding topographic and lateral force images, respectively, for linear upward and downward frequency sweeps between 350 and 370 kHz with a peak amplitude of 0.28 nm, corresponding to a drive voltage of 5V_p. At the beginning and at the end of image acquisition, no vibration was induced. It is observed that ripples become less pronounced or even disappear at the contact resonance frequency, depending on the drive voltage only, whereas for vibration frequencies away from the resonance, the ripple corrugation is slightly smaller than without external vibrations. Furthermore, darker areas, corresponding to lower friction, appear in the lateral force image in a range of frequencies $\Delta f \approx 8$ kHz around f_{res}. In Figure 4C,D, topography and corresponding lateral force images are shown for A_{exc} = 0.22 nm and in Figure 4E,F for A_{exc} = 0.14 nm at the same applied static load (984 nN). It is seen that at the lowest A_{exc}, ripples appear during the complete frequency scan; however, slightly darker areas, corresponding to lower friction (9% reduction), are observed in the corresponding lateral force images when the frequency is around f_{res} (362 kHz) in a range of $\Delta f \approx 4$ kHz. On the other hand, for the intermediate value of the excitation amplitude, ripples become less pronounced and much darker areas appear in the lateral force image, where the friction reduction is around 15%.

Finally, in Figure 5, we have plotted the ripple corrugation *versus* A_{exc} at $f = f_{res}$. Values were obtained by calculating one-dimensional FFT of the topography images. Amplitude of the ripples decreases up to A_{exc} = 0.28 nm (5V_p), where ripples disappear. The friction force average over the area is plotted as a function of A_{exc} in Figure 5. The friction diminishes up to $A_{exc} \approx$ 0.3 nm (6V_p) and levels off at a value around 150 nN, corresponding to a reduction of 42% compared with the absence of vibrations. Correspondingly, the effective friction coefficient decreases from about 0.57 to 0.34. The value obtained at the plateau is consistent with values reported on the macroscale for the silicon/polystyrene combination of materials in the absence of external vibrations.[27] It should be noted, however, that this coincidence must be considered fortuitous, because the reduction in friction observed in Figure 2 is even much larger than that and the friction coefficient in the presence of vibrations in this case is 0.08.

In order to investigate the kind of wear occurring in the present experimental situation, we have also imaged in dynamic mode an area previously scanned in contact with and without vertical vibrations (see Figure S1 in the Supporting Information). It is obvious from this figure that simultaneous application of a vibration amplitude of 0.55 nm at the contact resonance frequency completely suppresses ripple formation during scanning in contact mode. At the same time, the average height of the corresponding area is slightly higher than the pristine area not scanned previously in contact mode. This increase in average height is contrary to expectations based on the assumption of abrasive wear. Abrasive removal of material by the tip would also be evidenced by a significant pile up of material at the borders of the area scanned in contact mode, which is in contrast to the observations. We ascribe the apparent increase in height to surface roughening. This increased roughness of the sample after scanning in contact mode leads to interactions of the sidewalls of the tip with the rough sample. We have determined the root-mean-square (rms) roughness of the sample in a 2 × 2 μm^2 pristine area and in an area of the same size previously scanned in contact mode under the application of external vibrations with A_{exc} = 0.55 nm. The corresponding areas are indicated in Figure S1. The rms roughness is 0.32 nm for the pristine area and 1.35 nm for the area previously scanned in contact mode. This is very small compared with the roughening produced without external vibrations (rms on the order of 8 nm).

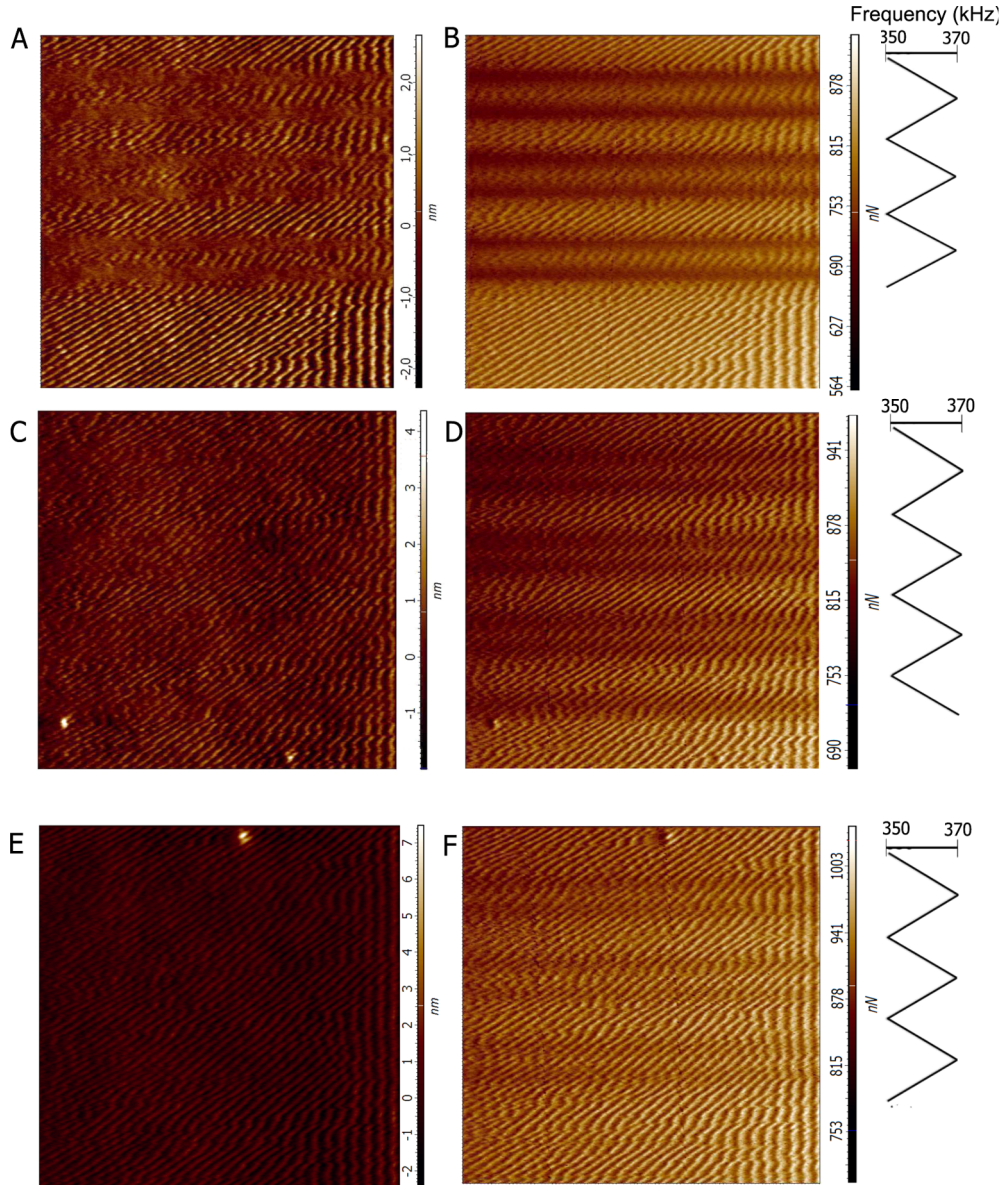

Figure 4. (A) Topography and (B) corresponding lateral force while scanning the external vibration frequency between 350 and 370 kHz (contact resonance frequency 362 kHz) with a peak excitation amplitude of 0.28 nm ($5V_p$). (C, D) Same as panels A and B, except with a peak A_{exc} of 0.22 nm ($4V_p$). (E, F) Same as panels A and B, but for a peak A_{exc} of 0.14 nm ($2.5V_p$). The diagrams on the right-hand side of the figures indicate the actual vibration frequency during the scan. Applied static load is 984 nN. Frame sizes: 10 × 10 μm^2.

DISCUSSION

The reduction of the rippling effect at increasing excitation amplitude has some interesting analogies with the reduction of friction, upon application of external vibration, observed in wearless stick–slip on the atomic scale.[12] The last effect is well interpreted by the so-called Prandtl–Tomlinson (PT) model.[11] In that case, the sharp tip of the AFM is elastically driven by the cantilever spring along a corrugated potential resembling the surface lattice. When the spring elongation reaches a critical value, the tip suddenly slips into a different location on the lattice. This process results in a sawtooth variation of friction versus time. When out-of-plane vibrations are applied while sliding, the energy barriers that the tip has to overcome are reduced. Correspondingly, the amplitude of the stick–slip pattern is also reduced, as well as the related friction force. In order to identify the stick–slip movement in the present case, we have studied the lateral force raw signal during scanning in contact mode with and without applied vibrations (see Figure S2 in the Supporting Information). While the stick–slip mechanism is not immediately evident from these signals, their derivatives exhibit a clear asymmetry when no vibrations are applied. This asymmetry disappears with increasing excitation amplitude. We ascribe the fact that the asymmetry is not much larger than observed here to the compliant nature of the polymer and to the circumstance that the tip is

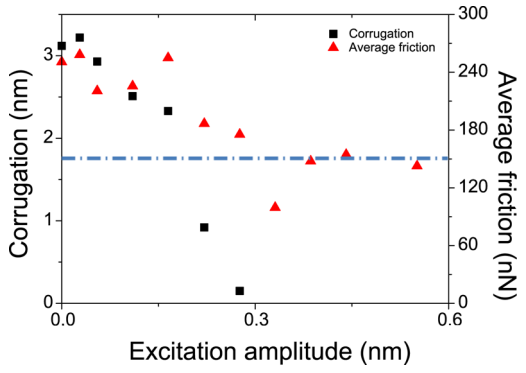

Figure 5. Corrugation as a function of the induced vertical peak excitation amplitude, A_{exc}, of the piezoelectric transducer from 0 nm (no vibration) to 0.55 nm ($10V_p$) at the contact resonance frequency (left-hand axis). Average frictional force (average value for both scan directions) as a function of A_{exc} from 0 nm (no vibration) to 0.55 nm ($10V_p$) at the contact resonance frequency (right-hand axis). Applied static load is 442 nN.

always at least in partial contact with the sample. It is clear from Figure S2 that the tip is not moving freely at any particular moment during the periodic external vibration.

In the present case, we can assume that the polymer surface, when the tip starts sliding, is essentially flat. However, the applied normal force (on the order of 1 μN) is enough to deform the substrate plastically. If the sliding velocity is low, a dimple surrounded by piled-up material is formed, which represents the beginning of the rippling process. While the tip sinks into the polymer, the depth and width of this dimple increase with time; at the same time the tip is pulled laterally by the increasing spring force (see Supporting Information Figure S3). Assuming that the evolving surface profile is associated with a similarly evolving surface potential, the analogy with the PT model allows us to conclude that, at a certain lateral force, the tip will suddenly hop across the piled-up material and repeat the same process at a new location in the pulling direction. Since the load and the velocity dependence of this process has been studied elsewhere,[28] in the rest of the discussion, we only focus on the influence of the mechanical vibrations.

When the piezoelectric element vibrates up and down, the normal force increases and decreases cyclically. On a rigid surface, this leads to a premature slip of the tip, as discussed in ref 11. On a compliant surface, the surface profile created by the tip is expected to partially follow the excitation amplitude, but only while the tip sinks into the polymer. When the tip retracts from the surface during the rapid oscillation, the normal force and therefore also the friction is strongly reduced because of the partly plastic response of the sample. This further facilitates the slip of the tip. Important contributions to this tip–sample interaction due to adhesion of the material during retraction can be excluded based on the force–distance curves acquired while indenting and completely removing the tip at arbitrary locations on the pristine substrate. As a result, the surface damage occurring in an oscillation cycle is reduced, which explains why the ripple corrugation diminishes with increasing excitation amplitude, A_{exc}. At the same time, the friction force decreases until it levels off at a value determined by the excitation amplitude and the normal load. This value can be smaller than the value given by the macroscopic friction coefficient.

A few remarks beyond this purely qualitative description apply, although a full theoretical analysis of wear reduction by mechanical vibrations, taking into account specific material properties is beyond the scope of the present study. At small deformations, the indenting tip causes an elastic deformation of the polymer, which can be approximately described by Hertz theory.[29] For a tip much harder than the sample, as in the present case, the penetration depth δ follows the relation $\delta^{3/2} \propto \frac{1-\nu^2}{E}\frac{1}{\sqrt{R}}F_N$, where E and ν are Young's modulus and Poisson's ratio of the sample, R is the radius of the tip, and F_N is the loading force. For polystyrene, the elastic modulus has been determined by nanoindentation experiments[26] as $E \approx 3.5$ GPa. This value is very close to the value $E \approx 3.4$ GPa calculated from the ultrasonic data of ref 30 acquired at an ultrasonic frequency of 2.25 MHz. In addition, for very thin films on substrates, the effects of the substrate must in principle be taken into account (see the review ref 31 and references contained therein). When the deformation exceeds a certain value, the stress–strain relation becomes nonlinear within the sample volume under the tip. When the stress reaches the yield stress, σ_y, plastic deformation begins, where the stress–strain relation exhibits hysteresis and which is more usefully characterized by a stress–strain rate relation instead of a stress–strain relation. Plasticity below the glass transition temperature, T_g ($T_g = 100$ °C for high molecular weight polystyrene), is generally thought to be thermally activated leading to Arrhenius laws for the strain rate at a given stress at $T \ll T_g$.[32−34] In the case of amorphous glassy polymers, plastic deformation is frequently associated with disentanglement of molecular chains with energy barriers, which are associated mainly with intermolecular interactions at low strain rates and high temperatures,[34] but involve activation of the secondary β molecular relaxation processes at high strain rates and low temperature.[35] For polystyrene, a yield stress of 88.9 MPa has been determined at low strain rates.[36] Estimating the stress under the tip by $\sigma = F_N/(\pi a^2)$ and calculating the contact radius a according to Hertz theory as $a = (F_N A R)^{1/3}$ with $A = \frac{3}{4}(1-\nu^2)/E$ and the Poisson ratio of polystyrene ($\nu = 0.34$),[37] the given yield stress would be reached for a very small normal force, $F_N = 90$ pN. Under the conditions of the present experiments, there is therefore always a volume of plastically deformed polymer under

the tip. A more precise estimate would use, for example, von Mises' shear–strain energy criterion of yield[38] and apply this criterion to elastic strains calculated by numerical techniques. This is not required for the present discussion, however. Irreversible plastic deformation, in addition to being a necessary ingredient for ripple formation during scanning, clearly favors the stick–slip mechanism of ripple suppression by ultrasonic vibrations, as the normal and frictional forces are strongly reduced by this effect in the decompression phase of the oscillation. We have observed ripples in the present study for normal loads larger than about 100–200 nN, that means about 3 orders of magnitude larger than the estimate for the onset of plasticity given above. This is fully consistent with previous results in ref 28, where ripple formation was explained as the result of the competition between the plastic indentation and the elastic shear force exerted by the tip.

Using uniaxial compression stress–strain experiments up to strain rates of 5000 s^{-1}, it has been shown for a number of polymers that σ_y depends significantly on the strain rate and can be several times the value measured at low strain rates.[39] This dependence of σ_y can be derived from thermal activation laws[32,35,40] and, for high strain rates, has been related to thermal activation of secondary β molecular relaxation processes.[41] The increase in the yield strength at high strain rates may contribute to the observed reduction of wear under external normal vibrations, in addition to the stick–slip mechanism outlined above. An order of magnitude estimate of the oscillatory strain rate is given by $\frac{A_{vib}}{d}\,\omega \approx \frac{10\,nm}{400\,nm}\,2\pi(360\ kHz) \approx 56000\ s^{-1}$, where A_{vib} is the vibration amplitude, amplified by the resonance and almost completely related to plastic and elastic deformation of the sample, d is the thickness of the sample, and ω is the angular contact resonance frequency. The present strain rates are hence at or beyond the upper limit of those investigated by Richeton *et al.*[39] (for other polymers). Therefore, a significant increase of the yield strength is indeed expected for the oscillatory deformation. Finally, it should be remarked that, because of the low thermal conductivity of polymers, the adiabatic heating effect during the compressional phase of the tip–sample vibration on the value of σ_y has to be considered. This effect would lead to a reduction of σ_y. The effect is, however, included in the measurements reported in ref 39, which, in addition, show a reduction of strain hardening in the plastic regime due to adiabatic heating.

CONCLUSIONS

To summarize, we have studied the effect of normal oscillations on the wear-induced nanopatterning of a polystyrene surface scanned by a sharp nanoindenter (corresponding to the tip of scanning force microscope) under high normal load. Wear, evidenced by the formation of ripples, is progressively reduced when external vibrations are applied at a frequency close to the contact resonance of the cantilever-tip–sample ensemble and when the amplitude, A_{exc}, of the external vibration increases. While performing the experiment, we have taken into account that the resonance frequency slightly changes with A_{exc}. The values of A_{exc} have been accurately calibrated by laser Doppler velocimetry. The effect of wear suppression (so-called "dynamic superlubricity") is reversible, indicating that the tip is not damaged by the vibrations. Our results suggest a possible method for "switching" AFM nanopatterns, generated by means of a scanning force microscope, on and off while scanning. They also confirm resonant contact vibrations as an efficient method to strongly reduce wear on the nanoscale. This has been shown here for the case of wear in the form of ripple formation on compliant materials but is expected to apply also to abrasive wear on the nanoscale for noncompliant materials or for higher normal forces. The observed effect is particularly interesting in applications to microelectromechanical systems (MEMS) operated in clean environments where fluid lubrication is not a feasible option. The contact resonance merely amplifies the vibration amplitude and vibrations of the same amplitude at other frequencies should be similarly effective. The contact resonance, however, enables control of wear at very small transducer amplitudes.

We may also ask how the present results can be extended to larger contacting surfaces, since this would enable extremely important practical applications. To this end, we first note that the interface between two engineering surfaces is usually not flat but rather formed by a multitude of micro- and nanojunctions that are continuously established and ruptured (*e.g.*, see ref 42). Plastic yield is known to be an important factor in this process. As shown above, ultrasonic vibrations can strongly reduce wear as evidenced by the formation of ripples, and the effect of these vibrations is strongly enhanced by the contact resonance. Due to the distribution of roughness over a wide range of length scales, contact resonances are spread over a wide frequency interval and will, in addition, also depend on the applied load (see also ref 43). Small scale asperities, however, are expected to dominate the contact mechanics,[42] and therefore the corresponding higher contact resonance frequencies should be more relevant for friction and wear. Many parameters are involved in the problem, including the geometric distribution of asperities on the two surfaces. Furthermore, the contact resonance spectrum may change with time, due to the plastic yield of small scale asperities. As a result, the problem seems to be very difficult to investigate in a quantitative way. Studying the effect of controlled vibrations on the contact mechanics of well-defined nanopatterned

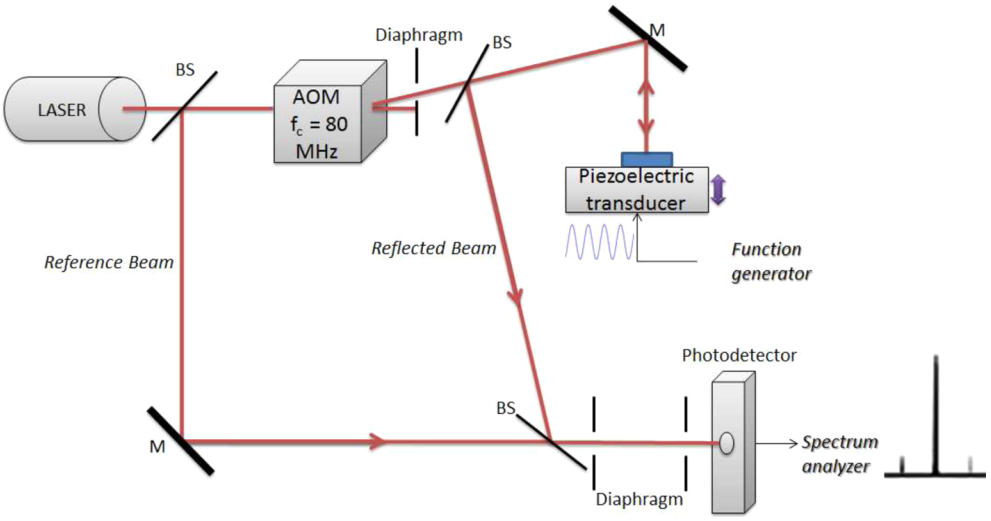

Figure 6. Laser Doppler velocimetry setup used for calibrating the out-of-plane excitation amplitude of the sample surface when excited by the piezoelectric transducer. The beam of a 632.8 nm HeNe laser is split into a reference beam and a beam that is diffracted by an acousto-optic modulator (AOM, carrier frequency 80 MHz) and then reflected by the sample. Both beams are recombined at a photodiode using a beam splitter. The electric signal from the photodiode is then Fourier transformed to detect sidebands of the 80 MHz carrier caused by the vibration of the sample. M, Mirror, BS, Beam Splitter.

surfaces (such as those produced by nanoimprinting or FIB) will constitute a useful step to clarify these issues. In conclusion, the study of surface rippling using ultrasonic AFM appears a very promising tool to characterize nonlinear elastic properties and plastic yield on the nanoscale and a good starting point to explore similar phenomena on complex surfaces of engineering interest.

EXPERIMENTAL SETUP

Sample Preparation. Thin films (thickness about 400 nm) were prepared by spin-coating (3000 rpm, 60 s) dilute solutions of atactic polystyrene (325 000 g/mol, PDI < 1.02, Polymer Source) in toluene (Merck 99.9%, HPLC grade) onto silicon wafers covered by a native oxide layer (around 2 nm). To allow fast ripple formation, the samples were used as spin-coated.

AFM Measurements. The ripples were produced by scanning in contact mode with a scan rate of 10 μm/s (0.5 scan lines/s) at ambient conditions with a commercial AFM system (Ntegra Prima, NT-MDT). Rectangular AFM silicon cantilevers FMG01 (NT-MDT) with silicon tips were used in all the experiments. Their nominal spring constant is between 1.2 and 6.4 N/m, and the typical tip radius is 10 nm. The cantilevers exhibit free resonant frequencies between 47 and 76 kHz. When the tip contacts the surface, the corresponding lowest bending resonance frequency has values in the range of 250−450 kHz, in accordance with previous studies.[44] The normal spring constant was precisely determined by thermal noise,[45] and lateral forces were calibrated using standard continuum mechanics.[46] To investigate the dependence of friction on out-of-plane vibrations, the sample was mounted on a highly damped piezoelectric transducer (compare Supporting Information Figure S4) driven directly by a sine signal supplied by an external function generator (model DDS 4030, PeakTech) or, alternatively, by one of the signal generators of the AFM.

Piezoelectric Transducer Calibration. Absolute calibration of the excitation amplitude has been performed in the present study by means of a home-built laser Doppler vibrometer (Figure 6). This tool allows the measurement of solid surface velocities based on the Doppler shift

$$\Delta f = \frac{2v/c}{1+v/c} f \approx \frac{2v}{\lambda} \quad (1)$$

of the frequency of light backscattered from a moving object. Here, v is the velocity component normal to the surface, and λ is the optical wavelength. The frequency modulation imposed on the light by a vibration of the reflecting surface is shifted down to measurable frequencies by interfering the reflected light with a reference beam at the photodetector. An acousto-optic modulator (AOM) in one of the beams shifts the modulation to the carrier frequency of the AOM and allows both side bands of the frequency-modulated signal to be observed. The amplitude of vibration is derived from the ratio of the side band and carrier amplitudes, a_1 and a_0, in the FFT of the signal

$$\left|\frac{a_1}{a_0}\right| = \left|\frac{J_1(\beta)}{J_0(\beta)}\right| \quad (2)$$

where J_0 and J_1 are Bessel functions of the first kind and β is the modulation index

$$\beta = \frac{\Delta f}{f_m} = \frac{2v_0/\lambda}{f_m} = \frac{4\pi x_0}{\lambda} \quad (3)$$

with $v_0 = 2\pi f_m x_0$; x_0 is the vibration amplitude and f_m is the frequency of vibration of the piezoelectric transducer. Only the first sidebands have been considered here, because the modulation index turns out to be small in the present case.

Using the home-built Doppler vibrometer, the calibration yielded a peak excitation amplitude of 0.55 ± 0.05 nm for a peak drive voltage of 10 V. The error results from unequal amplitudes of the lower and upper side bands used for the calibration. We also confirm that A_{exc} of the piezoelectric transducer is proportional to the applied ac voltage and that A_{exc} at a given drive voltage does not vary within the error of measurement within the frequency range used in the experiments described herein.

Conflict of Interest: The authors declare no competing financial interest.

Acknowledgment. The Spanish Ministry of Economy and Competitiveness (Project No. MAT2012-38810) is gratefully

acknowledged for financial support. We also thank Dr. Simone Napolitano for providing the PS sample.

Supporting Information Available: The Supporting Information is available free of charge on the ACS Publications website at DOI: 10.1021/acsnano.5b02466.

Supplementary figures and extended material section (PDF)

REFERENCES AND NOTES

1. Urbakh, M.; Klafter, J.; Gourdon, D.; Israelachvili, J. The Nonlinear Nature of Friction. *Nature* **2004**, *430*, 525–528.
2. Fridman, H. D.; Levesque, P. Reduction of Static Friction by Sonic Vibrations. *J. Appl. Phys.* **1959**, *30*, 1572–1575.
3. Akay, A. Acoustics of Friction. *J. Acoust. Soc. Am.* **2002**, *111*, 1525–1548.
4. Eaves, A.; Smith, A.; Waterhouse, W.; Sansome, D. Review of the Application of Ultrasonic Vibrations to Deforming Metals. *Ultrasonics* **1975**, *13*, 162–170.
5. Dong, S.; Dapino, M. J. Wear reduction through piezoelectrically-assisted ultrasonic lubrication. *Smart Mater. Struct.* **2014**, *23*, 104005.
6. Godfrey, D. Vibration Reduces Metal to Metal Contact and Causes an Apparent Reduction in Friction. *ASLE Trans.* **1967**, *10*, 183–192.
7. Bowden, F. P.; Tabor, D. *Friction: An Introduction to Tribology*; Anchor Press: Garden City, NY, 1973.
8. Dong, S.; Dapino, M. J. Elastic-Plastic Cube Model for Ultrasonic Friction Reduction Via Poisson Effect. *Ultrasonics* **2014**, *54*, 343–350.
9. Teidelt, E.; Starcevic, J.; Popov, V. Influence of Ultrasonic Oscillation on Static and Sliding Friction. *Tribol. Lett.* **2012**, *48*, 51–62.
10. Hesjedal, T.; Behme, G. The Origin of Ultrasound-Induced Friction Reduction in Microscopic Mechanical Contacts. *Trans. Ultrason. Ferroelectr. Freq. Control* **2002**, *49*, 356–364.
11. Socoliuc, A.; Gnecco, E.; Maier, S.; Pfeiffer, O.; Baratoff, A.; Bennewitz, R.; Meyer, E. Atomic-Scale Control of Friction by Actuation of Nanometer-Sized Contacts. *Science* **2006**, *313*, 207–210.
12. Gnecco, E.; Socoliuc, A.; Maier, S.; Gessler, J.; Glatzel, T.; Baratoff, A.; Meyer, E. Dynamic Superlubricity on Insulating and Conductive Surfaces in Ultra-High Vacuum and Ambient Environment. *Nanotechnology* **2009**, *20*, 025501.
13. Roth, R.; Fajardo, O. Y.; Mazo, J. J.; Meyer, E.; Gnecco, E. Lateral Vibration Effects in Atomic-Scale Friction. *Appl. Phys. Lett.* **2014**, *104*, 083103.
14. Lantz, M. A.; Wiesmann, D.; Gotsmann, G. Dynamic Superlubricity and the Elimination of Wear on the Nanoscale. *Nat. Nanotechnol.* **2009**, *4*, 586–591.
15. Aoike, T.; Uehara, H.; Yamanobe, T.; Komoto, T. Comparison of Macro- and Nanotribological Behavior with Surface Plastic Deformation of Polystyrene. *Langmuir* **2001**, *17*, 2153–2159.
16. Leung, O. M.; Goh, M. C. Orientational Ordering of Polymers by Atomic Force Microscope Tip-Surface Interaction. *Science* **1992**, *255*, 64–66.
17. Pickering, J. P.; Vancso, G. J. On the Formation of Oriented Nanometer Scale Patterns on Amorphous Polymer Surfaces Studied by Atomic Force Microscopy. *Appl. Surf. Sci.* **1999**, *148*, 147–154.
18. Yan, Y.; Sun, Y.; Yang, Y.; Hu, Z.; Zhao, X. Effect of the AFM Tip Trace on Nanobundles Formation on the Polymer Surface. *Appl. Surf. Sci.* **2012**, *258*, 9656–9663.
19. Schmidt, R. H.; Haugstad, G.; Gladfelter, W. L. Scan-Induced Patterning and the Glass Transition in Polymer Films: Temperature and Rate Dependence of Plastic Deformation at the Nanometer Length Scale. *Langmuir* **2003**, *19*, 10390–10398.
20. Napolitano, S.; D'Acunto, M.; Baschieri, P.; Gnecco, E.; Pingue, P. Ordered Rippling of Polymer Surfaces by Nanolithography: Influence of Scan Pattern and Boundary Effects. *Nanotechnology* **2012**, *23* (47), 475301.
21. Rabe, U.; Amelio, S.; Kester, E.; Scherer, V.; Hirsekorn, S.; Arnold, W. Quantitative Determination of Contact Stiffness Using Atomic Force Acoustic Microscopy Ultrasonics. *Ultrasonics* **2000**, *38*, 430–437.
22. Yuya, P. A.; Hurley, J. A.; Turner, D. C. Relationship Between Q-Factor and Sample Damping for Contact Resonance Atomic Force Microscope Measurement of Viscoelastic Properties. *J. Appl. Phys.* **2011**, *109*, 113528.
23. Rabe, U.; Kopycinska, M.; Hirsekorn, S.; Arnold, W. Evaluation of the Contact Resonance Frequencies in Atomic Force Microscopy As a Method for Surface Characterisation. *Ultrasonics* **2002**, *40*, 49–54.
24. Rupp, D.; Rabe, U.; Hirsekorn, S.; Arnold, W. Nonlinear Contact Resonance Spectroscopy in Atomic Force Microscopy. *J. Phys. D: Appl. Phys.* **2007**, *40*, 7136–7145.
25. Hopcroft, M. A.; Nix, W. D.; Kenny, T. W. What is the Young's Modulus of Silicon? *J. Microelectromech. Syst.* **2010**, *19*, 229–237.
26. Miyake, K.; Satomi, N.; Sasaki, S. Elastic Modulus of Polystyrene Film from Near Surface to Bulk Measured by Nanoindentation Using Atomic Force Microscopy. *Appl. Phys. Lett.* **2006**, *89*, 031925.
27. Bistac, S.; Ghorbal, A.; Schmitt, M. Friction of Polystyrene: Consequence on Nano-Wear. *Prog. Org. Coat.* **2006**, *55*, 345–354.
28. Gnecco, E.; Pedraz, P.; Nita, P.; Dinelli, F.; Napolitano, S.; Pingue, P. Surface Rippling Induced by Periodic Instabilities on a Polymer Surface. *New J. Phys.* **2015**, *17*, 032001.
29. Hertz, H. J. Uber die Berührurung Fester Elastischer Körper. *J. Reine Angew. Math.* **1881**, *92*, 156–171.
30. Kono, R. J. The Dynamic Bulk Viscosity of Polystyrene and Polymethyl Methacrylate. *J. Phys. Soc. Jpn.* **1960**, *15*, 718–725.
31. Oliver, W. C.; Pharr, G. M. An Improved Technique for Determining Hardness and Elastic Modulus Using Load and Displacement Sensing Indentation Experiments. *J. Mater. Res.* **1992**, *7*, 1564–1583.
32. Eyring, H. J. Viscosity, Plasticity and Diffusion As Examples of Absolute Reaction Rates. *J. Chem. Phys.* **1936**, *4*, 283–291.
33. Argon, A. S. A Theory for the Low-Temperature Plastic Deformation of Glassy Polymers. *Philos. Mag.* **1973**, *28*, 839–865.
34. Miehe, C.; Göktepe, J.; Méndez Diez, S. Finite Viscoplasticity of Amorphous Glassy Polymers in the Logarithmic Strain Space. *Int. J. Solids Struct.* **2009**, *46*, 181–202.
35. Richeton, J.; Ahzi, S.; Daridon, L.; Rémond, Y. A Formulation of the Cooperative Model for the Yield Stress of Amorphous Polymers for a Wide Range of Strain Rates and Temperatures. *Polymer* **2005**, *46*, 6035–6043.
36. Whitney, W.; Andrews, R. D. Yielding of Glassy Polymers: Volume Effects. *J. Polym. Sci., Part C: Polym. Symp.* **1967**, *16*, 2981–2990.
37. Rinde, A. Poisson's Ratio for Rigid Plastic Foams. *J. Appl. Polym. Sci.* **1970**, *14*, 1913–1926.
38. Johnson, K. L. *Contact Mechanics*; Cambridge University Press: Cambridge, U.K., 1985.
39. Richeton, J.; Ahzi, S.; Vecchio, K. S.; Jiang, F. C.; Adharapurapu, R. R. Influence of Temperature and Strain Rate on the Mechanical Behaviour of Three Amorphous Polymers: Characterization and Modeling of the Compressive Yield Stress. *Int. J. Solids Struct.* **2006**, *43*, 2318–2335.
40. Ree, T.; Eyring, H. J. Theory for Non-Newtonian Flow. I. Solid Plastic System. *J. Appl. Phys.* **1955**, *26*, 793–800.
41. Bauwens-Crowet, C. The Compression Yield Behaviour of Polymethyl Methacrylate over a Wide Range of Temperatures and Strain-Rates. *J. Mater. Sci.* **1973**, *8*, 968–979.
42. Persson, B. N. J. Contact Mechanics for Randomly Rough Surfaces. *Surf. Sci. Rep.* **2006**, *61*, 201–227.
43. Marinello, F.; Passeri, D.; Savio, E. *Acoustic Scanning Probe Microscopy*; Springer: Acoustic Scanning Probe Microscopy, 2013.
44. Rabe, U.; Janser, K.; Arnold, W. Vibrations of Free and Surface-Coupled Atomic Force Microscope Cantilevers: Theory and Experiment. *Rev. Sci. Instrum.* **1996**, *67*, 3281–3293.

45. Butt, M.; Jaschke, H. J. Calculation of Thermal Noise in Atomic Force Microscopy. *Nanotechnology* **1995**, *6*, 1–7.
46. Luthi, R.; Meyer, E.; Haefke, H.; Howald, L.; Gutmannsbauer, W.; Guggisberg, M.; Bammerlin, M.; Güntherodt, H. J. Nanotribology: an UHV-SFM Study on Thin Films of C_{60} and AgBr. *Surf. Sci.* **1995**, *338*, 247–260.